International Journal of Advanced Research in Engineering and Technology (IJARET)
Volume 10, Issue 2, March- April 2019, pp. 1-13, Article ID: IJARET_10_02_001
Available online at http://www.iaeme.com/IJARET/issues.asp?JType=IJARET&VType=10&IType=02
ISSN Print: 0976-6480 and ISSN Online: 0976-6499

TUNING THE OPTICAL AND MECHANICAL PROPERTIES OF Y_2O_3 CERAMICS BY THE INCLUSION OF La^{3+} ION IN THE MATRIX FOR INFRARED TRANSPARENT WINDOW APPLICATIONS

Mathew C.T
EMRL, Department of Physics, Mar Ivanios College,
Thiruvananthapuram, Kerala, India

ABSTRACT

Infrared transparent windows are generally used to protect highly delicate infrared sensor circuits from the harsh environments. In the present work a combustion technique was effectively used to incorporate La^{3+} ion in the yttria matrix. The crystallites were in the size limit of 20 nm. Powder characterization using X-ray diffraction, HRTEM and FTIR spectroscopy revealed that the La^{3+} ions were effectively replacing the Y^{3+} ion in the yttria matrix. There was a slight reduction in optical band gap with La^{3+} concentration. A novel sintering mechanism was used for sintering the samples by coupling definite proportions of resistive heating and microwave heating. The highly dense pellets showed better transmittance and hardness properties, which improved with La^{3+}concentration. The present study authorises that combustion synthesis of the samples followed by resistive coupled microwave sintering can effectively be used to tune the optical and mechanical, properties of infrared transparent ceramics. Improving the transmittance properties without deteriorating the mechanical properties through the resistive coupled microwave sintering is the major highlight of this novel work.

Keywords: Combustion synthesis, Hardness, Infrared window, Resistive coupled microwave sintering

Cite this Article: Mathew C.T, Tuning the Optical and Mechanical Properties of Y2O3 Ceramics by the Inclusion of La3+ Ion in the Matrix for Infrared Transparent Window Applications, *International Journal of Advanced Research in Engineering and Technology*, 10 (2), 2019, pp 1-13.
http://www.iaeme.com/IJARET/issues.asp?JType=IJARET&VType=10&IType=2

1. INTRODUCTION

Infrared transparent ceramics are materials which allow electromagnetic radiations in the infrared range to pass through them without being much scattered or absorbed. The studies on transparent ceramics was triggered by the invention of commercially successful translucent α-

Al_2O_3 which was used as the envelope of high pressure Na-vapour lamp by General Electric under the trade name Lucalox in 1966 [1]. In electronic industry it found applications as it is used to protect highly delicate infrared sensor electronic circuits from the harsh environments. Infrared inspection ports and infrared cameras employ the transmittance property of the infrared transparent ceramics in the mid infrared range [2]. Infrared transparent window is one among the indispensable parts of homing missiles.

Yttria is considered to be one of the most promising candidates among all infrared transparent windows. It has remarkable optical properties but the hardness is at a moderate level compared to other window materials [3,4]. It is reported that the substitution of heavier ions in the yttria matrix effectively improves the mechanical and transmittance properties [5]. Y_2O_3 and La_2O_3 both have 16 formula units per unit cell and no lattice distortions are expected in $La_xY_{2-x}O_3$ up to a value x=0.24 [6,7]. There are reports that even at ~1900^oC the cubic phase of yttria with 16 mole percent of La is stable [8,9]. The phase change for 9 mole percent lanthanum doped yttria occur only after 2325 K [6]. Moreover it is reported that La^{3+} is an effective sintering aid which enhance the transmittance properties of infrared transparent windows [10].

Sintering of the transparent ceramics to high density without much grain growth is a major challenge in the fabrication of infrared transparent windows used as infrared sensor protective dome in homing missiles [11]. For pure nano crystalline yttria powder, the sintering temperature is above 1600 ^oC. Recently our research team has developed a new sintering strategy which effectively couple the conventional resistive heating and microwave heating in definite proportion to reduce the sintering temperature and soaking duration [12]. The yttria pellets sintered using the novel method showed better transmittance properties in the UV-Visible and mid-infrared region. Even a reduction in sintering temperature and soaking duration reduces the grain size to a great extent which improves the hardness and transmittance properties. The presence of La^{3+} ion in the yttria matrix is reported to reduce the sintering temperature to ~1500 ^oC [13]. La^{3+} ions enhance the grain boundary mobility of yttria and it is the reason behind improved sinterability [14]. In addition to this the La^{3+} ions easily dissolves in the cubic lattice of yttria and reduce the grain growth [5,15]. Two step sintering mechanisms and high pressure sintering mechanisms were effectively used for sintering La doped yttria, but the transmittance is less than 80% [16]. Recently Gan et al. used hot pressing sintering to achieve a density of 99.9 % in 12 atom percent La doped yttria ceramics which showed a transmittance of 68.9 % at 400 nm and 81.9 % at 1100 nm where as a pellet sintered without applying pressure achieved 99.8 % of the theoretical density [17,18]. But no much work have so far been reported in this system, may be due to the difficulty in the sintering of the samples at low temperatures with reduced grain size and porosity.

In the present work we discuss in detail the synthesis of $La_xY_{2-x}O_3$ by a modified combustion route. Various powder characterisation techniques like X-ray diffraction, Transmission Electron Microscopy, Fourier Transform Infrared Spectroscopy and UV-Visible spectroscopy used to analyse the quality of the powder are discussed in detail. The optical and hardness properties of the samples sintered via resistive coupled microwave sintering are also described in detail.

2. MATERIALS AND METHODS

A single step auto-igniting combustion technique was used to synthesize nano structured $La_xY_{2-x}O_3$. Stoichiometric amount of high purity $Y(NO_3)_3.6H_2O$ (99.99 %, Alfa Aesar, USA) dissolved in double distilled water was mixed with La_2O_3 (99.99 %, Alfa Aesar, USA) dissolved in nitric acid, to make a clear solution. Citric acid was added to the precursor solution which act both as fuel and the complexing agent [11]. By adjusting the nitric acid and

ammonium hydroxide the pH of the precursor solution is made ~7. Nitric acid in the precursor solution reacts with the ammonium hydroxide forming ammonium nitrate which acts as the extra oxidant. The precursor solution was heated using a hot plate at 250 ^{o}C in a combustion chamber. On persistent heating, the solution foams and finally ignites giving voluminous and fluffy product of combustion.

X-ray diffractometer (X'pert pro, PANalytical, the Netherlands) with Cu Kα radiation in the range of 20–60º was used for the determination of crystalline structure and phase of the as prepared sample. The X-ray diffraction data was utilised for estimating the crystallite size via Scherrer's equation and Williamson-Hall plot. High resolution transmission electron microscopy (JEM-2100, JEOL, USA) operating at 200 kV was used for verifying the particulate properties and the crystallite size distribution. Fourier Transform Infrared spectrometer (Spectrum 2, Perkin-Elmer, Singapore) with diamond ATR in the range 400-4000 cm^{-1} was used to verify the phase purity of the as prepared sample. The absorption spectrum of as-prepared samples of were recorded using a spectrophotometer (UV-1700, Shimadzu, Japan).

The as prepared powder was uniaxially compacted into pellets in a 14 mm diameter steel die at 20 MPa using a hydraulic press. A novel resistive coupled microwave sintering technique was used for sintering the samples. The resistive coupled microwave furnace (VBCC/HMF/71, VB Ceramics Consultants, India) effectively couples the resistive heating and microwave heating in desired proportion. A pair of molybdenum disilicide heating elements was used for resistive heating and a pair of 2.5GHz magnetrons with power 1.1 kW each provides microwave heating support. The effective control over the heating rate and uniformly distributed fast heating cycles yield high quality infrared transparent ceramics with enhanced properties. By varying the percentage composition of the microwave and resistive powers the micro structure and the properties of the sintered samples can be tuned. In the present work, after a series of trials the resistive and microwave heating were effectively coupled in the ratio 60:40 below 1100 ^{o}C and there after it was fixed at 40:60.

Archimedes principle was used to find the experimental density of the sintered samples. Coarse grinding, lapping and fine polishing are effectively utilised for optical quality surface finish. For a higher quality surface finish more intermediate sizes of abrasives are used and more material might be removed from each step. Fine grade diamond lapping and polishing pastes and fluids of 5 µm, 1µm, 0.5 µm, 0.25 µm and 0.1 µm were mainly used for this. Finally a float polishing mechanism was employed in which the work piece was submerged and rotated in a slurry of extra fine quality polishing powder in deionized water. The well-polished pellets were used for transmittance studies. The transmittance of radiation in the UV-Visible and in the IR range were measured using UV-Visible and FTIR spectrometers.

Vickers indenter method (HMV 2TAW, Shimadzu, Japan) was used for studying the hardness of the well sintered pellets. Various indentation loads P of 0.98, 1.96, 2.94 and 4.90 N were used for a duration of 14 s to study the load dependent hardness of the samples. If the hardness of the sample decreases with increase in load it is called positive indentation size effect (ISE) [19]. For detailed analysis a semi empirical relation called modified proportional specimen resistance (MPSR) model is used for studying the ISE behaviour in the sintered samples [20]. The hardness of the sample for different indentations were estimated using the relation

$$P = a_0 + a_1 d + a_2 d^2$$

Where P is the applied load, *'d'* is the indentation size, 'a_0', 'a_1' and 'a_2' are parameters obtained from curve fitting of the experimental results. Here *'a_0'* is the term related to the

residual stresses generated in the specimen surface, a_1 is a constant related to the proportional resistance of the specimen which is directly proportional to the Young's modulus and 'a_2' is a constant related to load independent micohardness. The load independent hardness called true hardness H_T can be obtained from 'a_2' by the relation

$$H_T = ka_2$$

Where *k* is a constant equal to 1.8544 for Vicker's indenter [21].

3. RESULTS AND DISCUSSION

X-ray diffraction technique was effectively used to analyze the phase purity of the sample. X-ray diffraction patterns of Y_2O_3 and $La_xY_{2-x}O_3$ (where x = 0.05,0.10,0.15, 0.20 and 0.25) are shown in Fig. 1. All the peaks correspond to the cubic phase of yttria and are indexed using JCPDS file no-895591. No additional peaks were observed in the XRD pattern, which clearly indicate that the La^{3+} ions are substituting Y^{3+} ions in the yttria cubic structure. The ionic radius of La^{3+} (1.032 $\overset{o}{A}$) is larger than that of Y^{3+} (0.90 $\overset{o}{A}$) ions [22]. As the La^{3+} concentration increases the diffraction peaks shift towards shorter 2θ side which attributes to the increase in d-spacing due to the substitution of bigger La^{3+} ion in the Y^{3+} sites [16, 23].

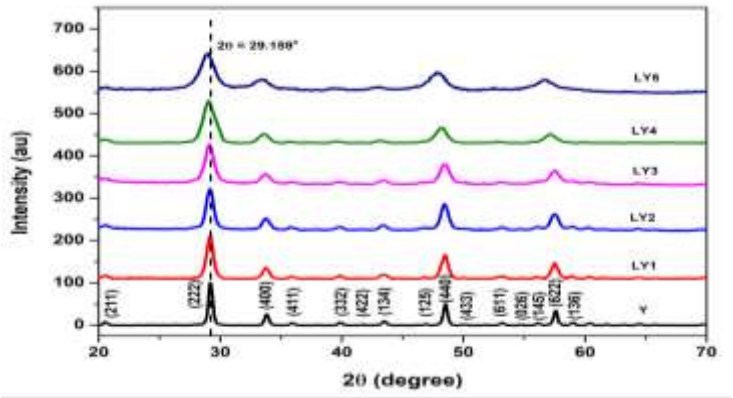

Figure 1 XRD pattern of $La_xY_{2-x}O_3$(where x= 0, 0.05,0.10,0.15,0.20 and 0.25)

Table 1 shows the variation in d-spacing and cell parameters for the (222) peak with increasing La^{3+} ion concentration. For convenience sample codes were assigned for each concentration and the crystallite sizes were calculated from the high intensity peaks using Scherrer formula.

The extent of line broadening in the diffraction pattern due to the strain, which is caused by the non-uniform displacement of the atoms with respect to their reference lattice position, could be identified by Williamson-Hall (W-H) method [24]. In this method, the reciprocal peak width (β cos θ)/λ is plotted against the reciprocal lattice distance (4*sinθ)/λ*, and the resulting plot is fitted linearly. Fig. 2 shows the Wiliamson-Hall plot for the $La_xY_{2-x}O_3$ nanoparticles. The lattice strain is estimated from the slope of the graph and the reciprocal of Y-intercept gives the crystallite size. The lattice strain and crystallite sizes for $La_xY_{2-x}O_3$ with different La^{3+} ion concentration are calculated and included in table 1. It is noticed that as growth of $La_xY_{2-x}O_3$ is restricted by the substitution of La^{3+} ion leading to relatively small crystallite size as compared to pure yttria. Similar behavior is observed by many researchers in oxide systems on incorporation of bigger ions in the crystal lattice. The positive slope indicates that the strain developed is tensile in nature [25].

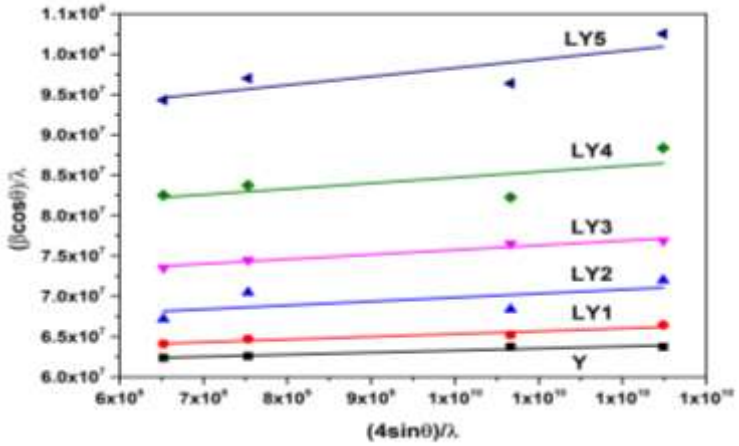

Figure 2 Williamson-Hall plot for $La_xY_{2-x}O_3$ with different La^{3+} ion concentration

Table 1 Variation in d-spacing and cell parameter with La^{3+} ion concentration

$La_xY_{2-x}O_3$	Sample Code	d-spacing (Å) for (222) plane		Crystallite size		Micro strain
		JCPDS file 895591	Present Sample	Scherrer Formula	W-H plot	
x = 0	Y	3.0615	3.0601	14.16 ± 0.20	16.30	2.17×10^{-4}
x= 0.05	LY1	3.0615	3.0639	13.20 ± 0.14	16.1	2.50×10^{-4}
x= 0.10	LY2	3.0615	3.0657	12.16 ± 0.23	15.4	4.91×10^{-4}
x= 0.15	LY3	3.0615	3.0693	11.71 ± 0.25	14.2	5.73×10^{-4}
x= 0.20	LY4	3.0615	3.0722	10.68 ± 0.24	12.8	7.15×10^{-4}
x= 0.25	LY5	3.0615	3.0767	9.74 ± 0.23	11.4	1.08×10^{-3}

There is a linear relationship between the La^{3+} concentration and lattice constant in the yttria matrix as shown in Fig. 3. A graph is plotted with the lattice constant (a) with the concentration of La^{3+} concentration (C) and is linearly fit according to the relation $a = 10.602 + 0.0105C$. It is found that lattice constant changes from 10.613 to 10.658 Å as the La^{3+} concentration changes from 1 mole % to 5 mole % .

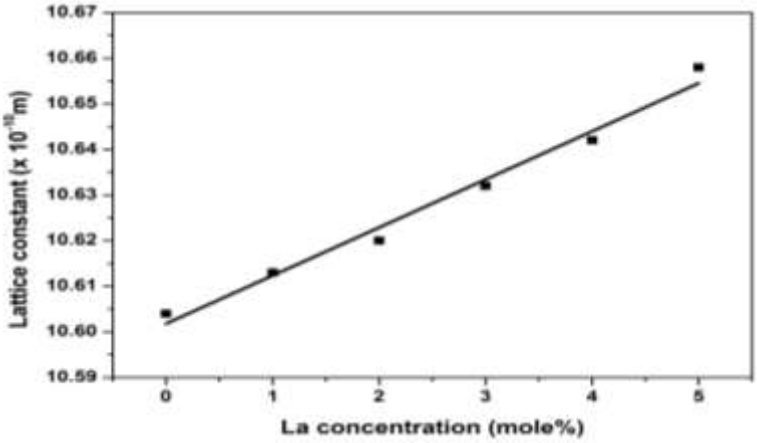

Figure 3 Variation in cell parameter with La^{3+} ion concentration

The crystallite size distribution from the TEM image of the as prepared LY3 sample which is shown in the Fig. 4 supports the XRD results. The crystallite size are found to be in the range 7 - 24 nm. Maximum number of crystallites lie in the size range 10 -12 nm and the

average crystallite size for the entire distribution is calculated as 11.58 ± 0.33nm. Fig. 5 shows the HRTEM image of the as prepared LY3 powder sample. The crystallographic planes are well defined and they are in good agreement with the XRD data.

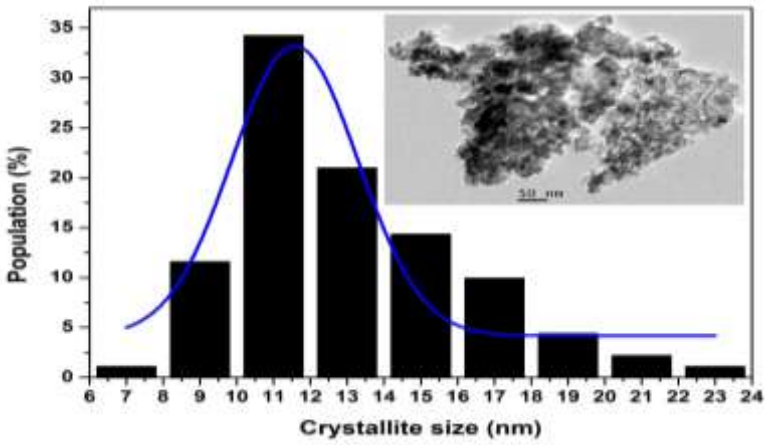

Figure 4 Crystallite size distribution of as prepared LY3. TEM image is shown inset.

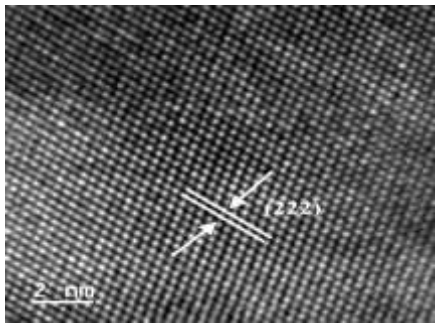

Figure 5 HRTEM image of as synthesized LY3 sample

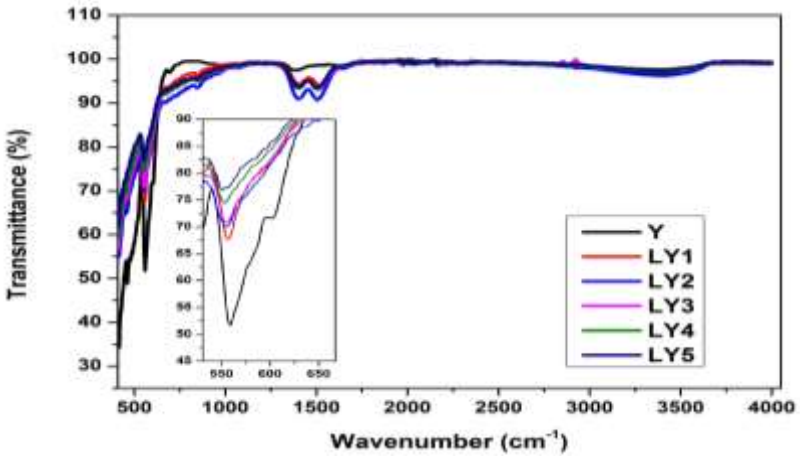

Figure 6 FTIR spectrum of as synthesized $La_xY_{2-x}O_3$. The characteristic peak for different compositions are shown in the inset

The chemical and structural information for identifying and characterizing the nanopowders are further studied using FTIR spectra. The FTIR spectra shown in Fig. 6 confirms that the $La_xY_{2-x}O_3$ powder transmits in the mid IR range. The absorption peak at 559 cm^{-1} is assigned to Y-O stretching in the case of pure yttria [26]. In the present sample there is a slight shifting of this peak to longer wavelength range as reported in the literature [27]. But there is no additional peaks. From the XRD pattern it is clear that in the present composition

La^{3+} ions dissolves in the yttria matrix and there is no change in the phase, but there is a slight increase in the lattice parameter. ie as La^{3+} ion concentration increases the cell volume increases. With the increase in the cell volume the IR absorption peak shifts towards longer wavelength range [28]. The FTIR spectrum in figure 6 corroborate the results obtained from the XRD. Fig. 7 shows the variation in absorption wave number with cell volume.

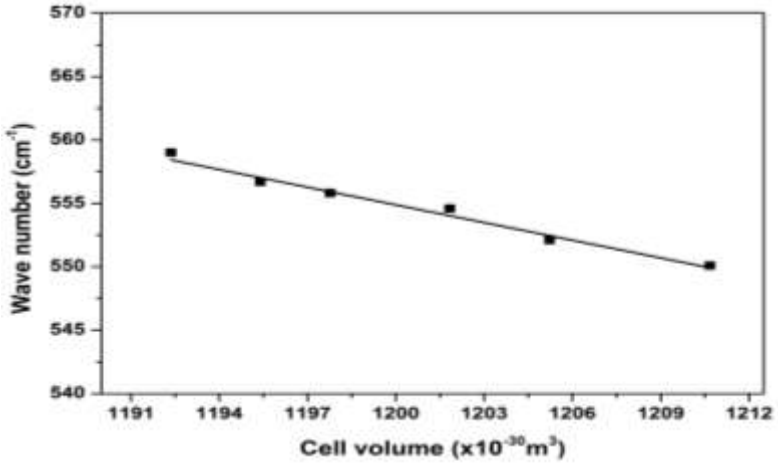

Figure 7 Variation in absorption wave number with cell volume

The high energy edge of a transparent ceramics is determined by the energy gap between the conduction and valence orbital band which is called the energy gap E_g [29]. The UV-Visible absorption spectrum was recorded in the range 200-800 nm and is shown in Fig. 8. The sample showed maximum absorption in the UV region and decreases towards the visible region. The wavelength corresponding to maximum absorption for the samples shifts towards longer wavelength range as La^{3+} ion concentration increases.

The measured reflectance is converted into Kubelka-Munk (K-M) function $F(R) = (1-R)^2 / (2R)$, where R is the reflectance. The K-M function is proportional to the absorption coefficient α in the Tauc equation [29]. Fig. 9 shows Tauc's plot in the form of Kubelka-Munk function of the optical absorption spectrum of yttria nanopowder. A graph is plotted with $(F(R)*h\upsilon)^2$ against the energy hυ of the incident photon and the optical band gap energy obtained from the intercept of the linear region with the energy axis at $(F(R)*h\upsilon)^2 = 0$. It is observed that with La^{3+} addition the band gap gradually decreases 5.65eV of pure yttria to 5.51eV of sample LY5.

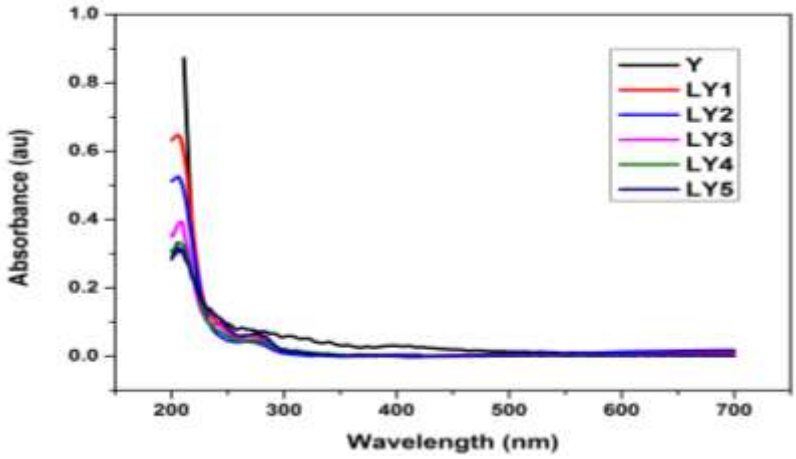

Figure 8 UV-Visible absorption spectrum of as synthesized $La_xY_{2-x}O_3$

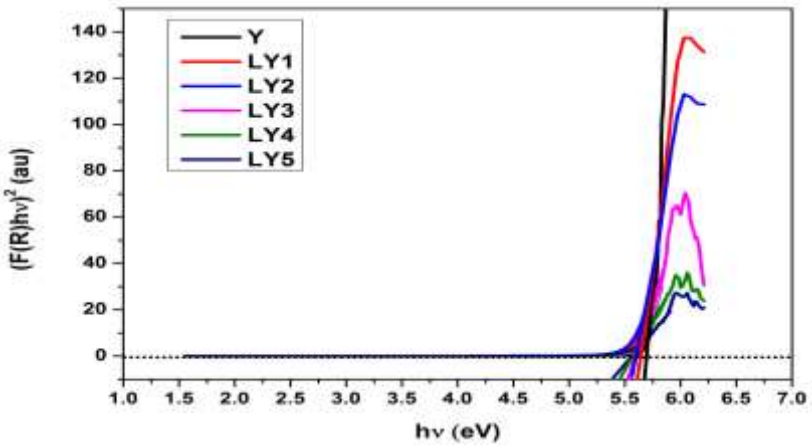

Figure 9 Tauc's plot of as synthesized $La_xY_{2-x}O_3$ in terms of Kubelka Munk function.

Table 2 Density achieved by the pellets of different composition

Sample Code	Sintering Temperature ($\pm 10\,^{o}C$)	Maximum relative density achieved (%)
Y_{RM}	1450	99.2 ± 0.01
$LY1_{RM}$	1440	99.2 ± 0.02
$LY3_{RM}$	1430	99.2 ± 0.02
$LY5_{RM}$	1430	99.1 ± 0.02

The $La_xY_{2-x}O_3$ nanopowder is uniaxially compacted into pellets in a 14 mm diameter steel die at 20 MPa using a hydraulic press. All the pellets were sintered using resistive coupled microwave heating showed high relative density >99% of the theoretical density. For a comparative study the samples Y, LY1, LY3 and LY5 sintered via resistive coupled microwave sintering were coded as Y_{RM},$LY1_{RM}$, $LY3_{RM}$ and $LY5_{RM}$ respectively and tabulated in table 2.

For a comparative study the transmittance of the pellets in the UV-Visible range with different La^{3+} ions sintered via resistive coupled microwave heating are used. The maximum transmittance of 80.5% is shown by the sample $LY5_{RM}$. The comparison of transmittance of different samples in the UV-Visible region are shown in Fig. 10.

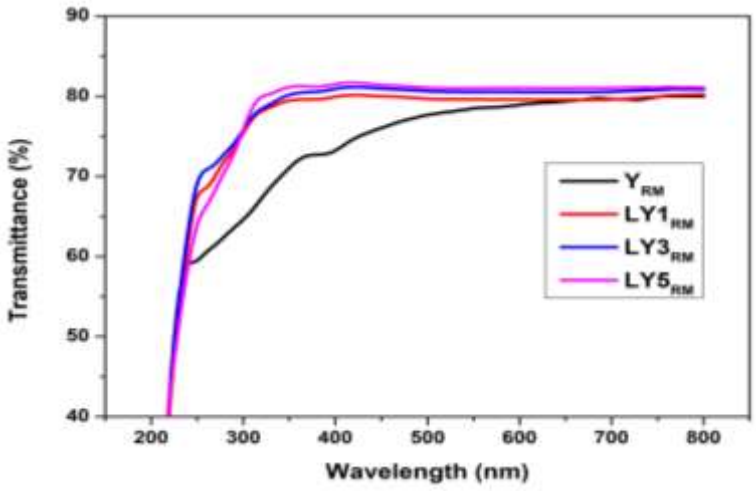

Figure 10 Transmittance percentage in the UV-Visible range in different pellets sintered using resistive coupled microwave heating

The transmittance properties of the pellets in the mid infrared range is studied. The upper IR cut off or the long wavelength edge of a transparent ceramics is determined by the energy absorption used for transition between the vibration states of the lattice called phonons. Usually the overtones of the principal lattice vibration define the upper IR cut off [11].

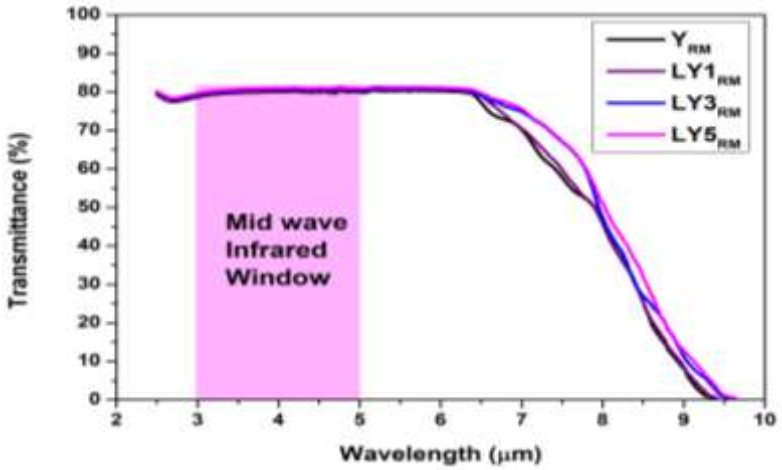

Figure 11 Transmittance percentage in the mid IR range in different pellets

The transmittance of radiations through the pellets with different La^{3+} ion concentration and sintered via resistive coupled microwave heating are studied. It is shown in Fig. 11. From the figure it is clear that as the concentration of La^{3+} ion increases there is a slight increase in the infrared cut off. Since ionic size of La^{3+} ion is greater than that of Y^{3+}, La-O fundamental phonon vibrational frequency is less than that Y-O so the phonon absorbing edge shifts towards the longer wavelength range [11]. Compared to pure yttria sintered via resistive coupled microwave heating, $La_xY_{2-x}O_3$ having a slight increase in the percentage transmittance. Fig. 12 shows the variation in dielectric constant with frequency for different samples.

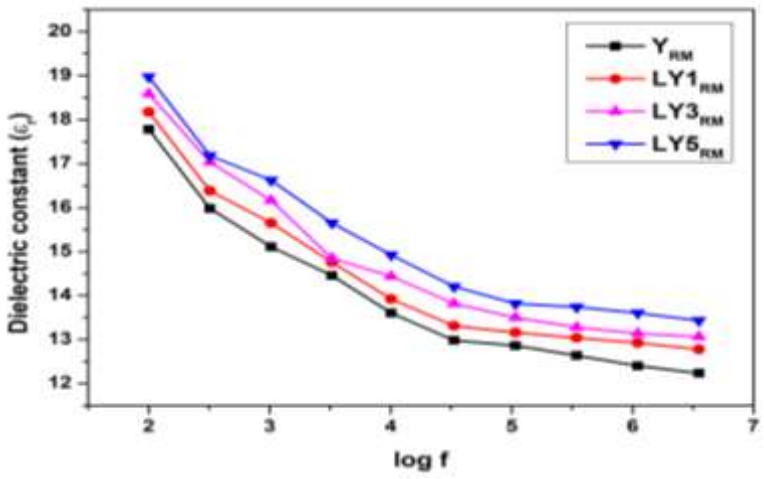

Figure 12 Variation in dielectric constant with frequency for different pellets

For the sample Y_{RM} the dielectric constant is found to be 12.23 and that for the sample $LY5_{RM}$ it is 13.48. The increase in transmittance in the UV-Visible region and mid-IR region may be due to the change in dielectric properties of the yttria matrix with La^{3+} ions. The variation of dielectric loss with frequency for different pellets are shown in Fig. 13. As in the case of pure yttria all other samples show a decrease in dielectric loss with temperature [30] .

But it is worth to note that the dielectric loss increases with the increase in La^{3+} concentration, which may be the reason behind the improved sinterability of La substituted yttria. In resistive coupled microwave sintering the green pellet absorbs the microwave energy generated by the magnetrons and convert it into heat within. The absorbed microwave power is proportional to the magnitude of electric field distribution in the sample. As the dielectric loss increases the microwave absorption in the sample increases [31]. In microwave sintering, the densification commences at a relatively low temperature by enhancing the diffusion mechanisms. So the sintering temperature and the soaking time can be reduced considerably. The microwave ponderomotive force induced mass transport is considered to be the reason behind the high densification in microwave sintering [32]. Even in low dielectric loss materials as temperature increases the dielectric loss factor increases and at higher temperatures they can effectively absorb the microwaves [33].

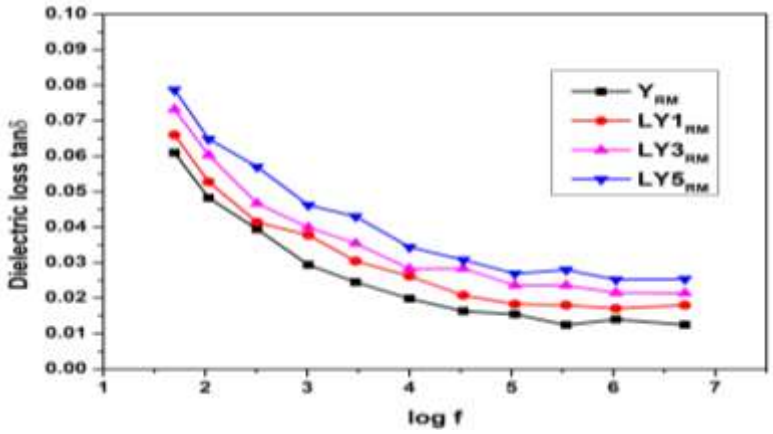

Figure 13 Variation in dielectric loss with frequency for different pellets

To analyse the load dependent hardness of the samples Y_{RM},$LY1_{RM}$, $LY3_{RM}$ and $LY5_{RM}$ MPSR model is used. Variation in indentation size with applied load for different La^{3+} concentration is shown in Fig. 15.

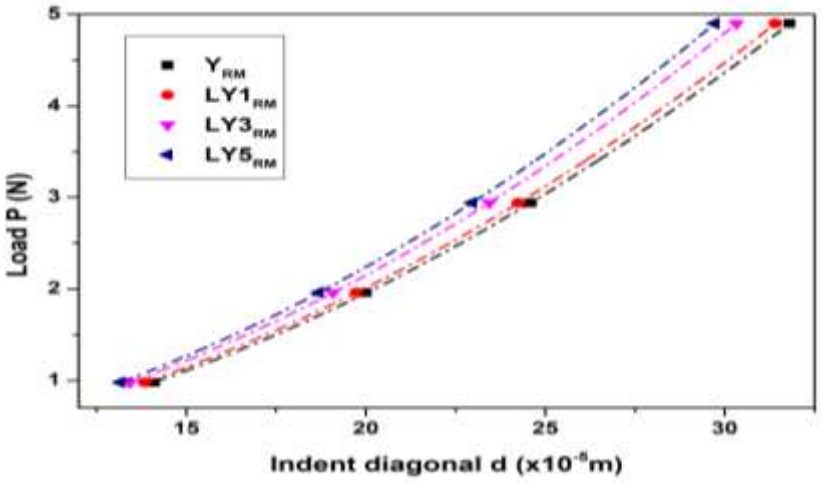

Figure 15 Variation in indentation size with applied load for different La^{3+} concentration

A P versus d graph is plotted for different compositions as in Fig 15 and the parameters obtained are tabulated in table 3. The results reveals that as the presence of La^{3+} ions in the matrix increases the hardness increases and maximum hardness of 10.05 GPa is shown by the sample $LY5_{RM}$.

Table 3 True hardness of $L_xY_{2-x}O_3$ pellets based on MPSR model.

Samples	a_0 **(N)**	a_1 **(N/μm)**	$a_2 = \frac{P_c}{d_0^2}$ **(N/μm²)**	H_T **(GPa)**
Y_{RM}	0.00064	0.00227	0.00477	8.85
$LY1_{RM}$	0.01011	0.00262	0.00487	9.03
$LY3_{RM}$	0.00182	0.00238	0.00525	9.73
$LY5_{RM}$	0.01638	0.00447	0.00542	10.05

3. CONCLUSIONS

The comprehensive analysis based on XRD and FTIR spectroscopy reveals that by the modified auto igniting combustion technique La^{3+} ion effectively substitutes Y^{3+} ions in the yttria matrix without changing the body centred cubic phase. In nanostructured $La_xY_{2-x}O_3$ (where x= 0, 0.05,0.10,0.15,0.20 and 0.25) powders the crystallites size analysis using Scherer formula reveals that at La^{3+} concentration increases crystallite size decreases. The TEM image analysis support the estimation of crystallite size and d-spacings obtained from XRD data. The crystallite size calculated for LY3 sample using XRD is 11.71 ± 0.25 nm and TEM is 11.58 ± 0.33nm. Williamson Hall plot is used to deconvolute the size and strain effect in XRD peak broadening which indicates that there is tensile strain in the crystallites which may contribute to peak broadening. As La^{3+} ion concentration increases the lattice strain increases due to difference in ionic size of La^{3+} and Y^{3+} ions. As La^{3+} ion concentration increases the cell volume increases but no phase changes are observed which attributes to the shift in absorption peak towards longer wavelength range in the FTIR spectrum. No additional peaks are observed in the spectrum which indicates that no impurities are present in the sample. The powder characterization conclude that nano crystalline phase pure yttria synthesized by the single step auto igniting combustion is stable at relatively high temperatures and transmit electromagnetic radiations in the UV-Visible and mid IR range. Pellet sintered via resistive coupled microwave heating showed high density, reduced grain size and minimum porosity, which attributes to the improved transmittance of 80% in the Uv-visible and 81% in the mid IR range. The studies on dielectric properties of the sample reveal that as La^{3+} ion concentration increases the dielectric constant and dielectric loss of the samples increase which attributes to the increased sinterability and improved transmittance. The microhardness of $LY5_{RM}$ is 10.05 GPa which is found greater than that of pure yttria. Thermal conductivity of the samples decreases with La^{3+} concentration. The results clearly indicate that the novel resistive coupled microwave sintering can effectively and economically be used to fabricate high quality infrared transparent windows and the presence of La^{3+} ion in the matrix considerably improves the hardness.

REFERENCES

[1] Goldstein A and Krell A, Transparent ceramics at 50: Progress made and Further Prospects, J. Am. Ceram. Soc., (2016) 1-25.

[2] Deborah D S and Aldo R B, “Industrial developments in the field of optically transparent inorganic materials: A survey of recent patents”, Rec. Pat. Mater. Sci., 1 (2008) 56-73.

[3] Serivalsatit K, Kokuoz B, Kokuoz B Y, Kennedy M and John B, Synthesis, Processing and Properties of Submicrometer-Grained Highly Transparent Yttria Ceramics, J. Am. Ceram. Soc., 93[5] (2010) 1320-1325.

[4] Tsukuda Y, Properties of blackY_2O_3 sintered bodies, Mater. Res. Bull., 16(1981) 453-459.

[5] Zhang L, Feng J and Pan W, *Vacuum sintering of transparent Cr:Y_2O_3 ceramics*, Cerami. Int., 41[7] (2015) 8755-8760.

[6] Troph W J and Harris D C, *Mechanical thermal and optical properties of yttria and lanthana-doped yttria,* Proc. SPIE., 1112 (1989) 9-19.

[7] Luo J M, Deng L P and Xu J L, *Fabrication of* $(Nd_{0.01}La_xY_{0.99-x})_2O_3$ *nanoparticles and Transparent ceramics by combustion synthesis,* J. Nanosci. Nanotechno., 11 (2011) 9705-9708.

[8] Horvath S F, Harmer M P, Williams D B, Notis M R,*Analytical transmission electron microscopy of La_2O_3 –doped Y_2O_3,* J. Mater. Sci., 24 (1989) 863-872.

[9] Wei G C, Emma T, Rhodes W H, Horvath S and Harmer M, *Analytical microscopy study of phases and fracture in Y_2O_3 - La_2O_3,* J. Am. Ceram. Soc., 71[10] (1998) 820-825.

[10] Li X, Mao X, Feng M, Qi S, Jiang B and Zhang L, *Fabrication of transparent La-doped Y2O3 ceramics using different La_2O_3 precursors,* J. Eur. Ceram. Soc., 36[10] (2016) 2549-2553.

[11] Harris D C, Materials for Infrared Windows and Domes, Properties and Performance. SPIE Press, Bellingham, WA, 1999.

[12] Mathew C T, Sam Solomon , Jacob Koshy and Jijimon K Thomas, *Infrared transmittance of hybrid microwave sintered yttria*, Ceram. Int., 41[8] (2015) 10070-10078.

[13] Yihua H, Liang J D, Xian Z J and Ling L Q, *Fabrication of lanthanum doped yttria transparent ceramics*, Chinese. Sci. Bull., 54 (2009) 2143-2146.

[14] Huang Y, Jiang D, Zhang J and Lin Q, *Precipitation synthesis and sintering of lanthanum doped yttria transparent ceramics,* Opt. Mater., 31 (2009) 1448-1453.

[15] Dong L M, Han Z D, Wu Z and Zhang X Y, *Preparation of $La_{0.1}Nd_{0.1}Y_{1.8}O_3$ nanopowders and characterisations of the optical properties,* Mater. Chem. Phys., 135 (2012) 575-578.

[16] Huang Y, Jiang D, Zhang J, Lin Q, *Fabrication of transparent lanthanum doped yttria ceramics by combination of two-step sintering and vacuum sintering,* J. Am. Ceram. Soc., 92[12] (2009) 2883-2887.

[17] Gan L, Park Y J, Zhu L L, Go S, Kim H, Kim J M and Ko J W, *Enhancement of the optical transmittance of hot-pressed transparent yttria ceramics by a multi-step sintering process,* Ceram. Int., 42[12] (2016) 13952-13959.

[18] Gan L, Park Y J, Zhu L L, Go S, Kim H, Kim J M and Ko J W, *Fabrication and properties of La_2O_3 doped transparent yttria ceramics by hot pressing sintering,* J. Alloy. Compd., 695(2017) 2142-2148.

[19] Durst K, Backes B, Franke O and Goken M, *Indentation size effect in metallic materials:Modeling strength from pop-in to macroscopic hardness using geometrically necessary dislocations,* Acta. Mater., 54 (2006) 2547-2555.

[20] Gong G, Wu J and Guan Z, *Load dependence of the apparent hardness of silicon nitride in a wide range of loads*, Mater. Let., 35[1-2] (1998) 58-61.

[21] Gong J and Li Y, *An energy-balance analysis for the size effect in low-load hardness testing,* J. Mater. Sci., 35 (2000) 209-213.

[22] Shannon R D, *Revised Effective Ionic Radii and Systematic Studies of Interatomic Distances in Halides and Chalcogenides,* Acta. Crystallogr. A, 32 (1976) 751-767.

[23] Mao X, Li X, Feeng M, Fan j, Jiang B and Zhang L, *Cracks in transparent La-doped yttria ceramics and the formation mechanism,* J. Eur. Ceram. Soc., 35 (2015) 3137-3143.

[24] Williamson G K, Hall W H, *X-Ray Line Broadening from Filed Aluminium and Wolfram,* Acta. Metall. Mater., 1 (1953) 22-31.

[25] Murugesan C, Chandrasakaran G, *Impact of Gd3+-substitution on the structural, magnetic and electrical properties of cobalt ferrite nanoparticles,* RSC Adv., 5 (2015) 73714-73725.

[26] Srinivasan R, Yogamalar R, and Bose A C, *Structural and optical studies of yttrium oxide nanoparticles synthesized by co-precipitation method,* Mat. Res. Bull., 45 (2010) 1165-1170.

[27] Thomas M E and Joseph R, *A comprehensive model for the intrinsic transmission properties of optical windows ,* Proc. SPIE., 929 (1988) 87-93.

[28] McDevitt N T and Davidson A D, *Infrared lattice spectra of cubic rare earth oxides in the region 700 to 50 cm^{-1},* J. Opt. Soc. Am., 56[5] (1966) 636-638.

[29] Kubelka P, *New Contributions to the Optics of Intensely Light-Scattering Materials Part I,* J. Opt. Soc. Am., 38 [5] (1948) 448-457.

[30] Chen J, Gao Z P, Wang J M and Zhang D H, *Dielectric properties of yttria ceramics at high temperature,* J.Elec.Sci.Tech.China., 5[4] (2007) 320-324.

[31] Ayappa K G, *Modelling Transport Process During Microwave Heating: A Review*, Rev. Chem. Eng., 13[2] (1997) 1-69.

[32] Rybakov K I and Semenov V E, *Mass transport in ionic crystals induced by the ponderomotive action of a high frequency electric field,* Phys. Rev. B., 52[5] (1995) 3030-3033.

[33] Katz J D, *Microwave sintering of ceramics,* Annu. Rev. Mater. Sci., 22(1992) 153-170.

[34] Gentilman R L, *Current and emerging materials for 3-5 micron IR transmission,* Proc. SPIE., 683 (1986) 2-11.